Mathematical Modeling of Fluidized-Bed Chlorination of Rutile

L. Zhou and H. Y. Sohn
Depts. of Metallurgical Engineering and of Chemical and Fuels Engineering, University of Utah, Salt Lake City, UT 84112

A mathematical model was formulated to describe the reaction rate and the particle size distribution of solids in a fluidized bed for the chlorination of rutile by a CO/Cl_2 mixture. The bubble assemblage model was applied to describe the gas behavior in the bed. The particle-size distribution in the bed was determined by a population balance. Predictions of the model gave satisfactory agreement with experimental results. The effects of important variables such as superficial gas velocity, exchange rate between the phases, and the reaction-rate constant were evaluated.

Introduction

Fluidized-bed processes have been used extensively in solid-catalyzed gas-phase reactions and gas–solid reactions. The chlorination of rutile to produce titanium tetrachloride, an intermediate in the production of titanium metal and titania pigment, is carried out in a fluidized bed. The main advantage of fluidized-bed processes are rapid mass and heat transfer, the ease of reactant material handling and control of operational conditions, uniform temperature, and good mixing throughout the bed.

Despite the widespread application of the fluidized bed in the production of titanium tetrachloride, its design and scale-up are still difficult. The main reason is the insufficient understanding of gas and solid movements in the bed. A fluidized bed can be operated in a particulate, bubbling, or turbulent fluidization mode. Different operating conditions result in different hydrodynamic behaviors of gases and solids in the bed. Therefore, a single set of principles cannot be applied to all modes of operation.

There have been many investigations to elucidate the phenomena involved in a bubbling-gas fluidized bed, and many models have been proposed to describe the gas and solid behaviors. The most widely accepted model is the two-phase model (Kato and Wen, 1969; Van Swaaij and Zuiderweg, 1972; Werther, 1978), in which a fluidized bed is pictured as consisting of a bubble phase that comes from the excess gas flow above the minimum fluidization velocity and an emulsion phase that is similar to the bed in incipient fluidization (Lapidus and Amundson, 1977). A number of different versions of the two-phase model have been proposed. Among them, the Kunii–Levenspiel model (Kunii and Levenspiel, 1991) incorporating the Davidson bubble and wake (Davidson et al., 1985) is most widely used. Along with the movement of gas in the fluidized bed, solid particles are dragged up as clouds or wakes by bubbles and descend by gravity in the emulsion phase. Fresh particles are fed continuously to the bed, and are discharged either through an overflow pipe or by entrainment of gases. Particle size and density may change in a noncatalytic reaction, and particles of the same size have different residence time in the bed. The elutriation rate depends on particle size. All of these must be accounted for in order to predict and control the behavior of the solids in a fluidized bed.

There are a number of investigations that report on the chlorination of titanium-bearing materials in the fluidized bed (Rhee and Sohn, 1990a, c; Harris et al., 1976). Several mathematical models have been developed to simulate the fluid dynamics and reaction phenomena in the bed (Kunii and Levenspiel, 1968; Bukur et al., 1974; Fuwa et al., 1978; Youn and Park, 1989; Rhee and Sohn, 1990b). Fuwa et al. (1978) introduced the bubble assemblage model to interpret the selective chlorination of oxidized ilmenite ore in the batch-type fluidized bed. Rhee and Sohn (1990b) developed a more detailed model that incorporates the solid mixing. Youn and Park (1989) developed a model to simulate the chlorination of rutile with coke in a fluidized bed.

In this work, the bubble assemblage model was used to describe the bed behavior with several new features. A particle size-dependent reaction-rate expression, which takes into account the particle-size distribution of the solid, was incorporated to calculate the concentration profile of reactant

Correspondence concerning this article should be addressed to H. Y. Sohn.

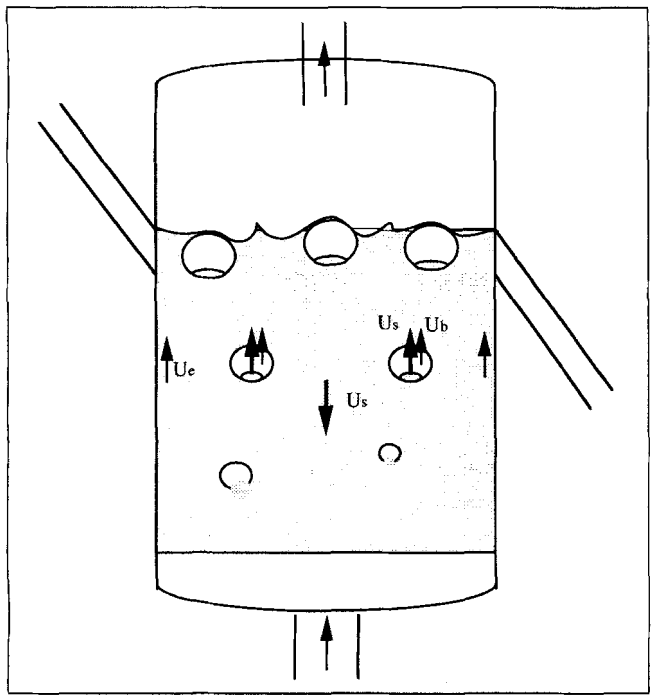

Figure 1. Fluidized bed.

gases in the bed. This rate expression is more realistic than those previously used (Fuwa et al., 1978; Youn and Park, 1989). The particle-size distribution in the bed was determined by a population balance. The model assumes that the solid particles are well mixed throughout the bed, but gas concentrations vary with the bed height. This makes the model applicable to industrial application where the concentrations of reactant gases may change substantially along the bed height. The experimentally determined intrinsic chlorination kinetics of rutile particles were used in this work.

Formulation of Model Equations

Figure 1 shows schematically a fluidized bed with the following features:

1. The bed consists of three regions: bubble, cloud, and emulsion. The gases are exchanged between these regions. Considering other uncertainties in the fluidized-bed model, such as the estimation of gas-interchange parameter and chemical kinetics, the description of the fluidized bed was simplified by neglecting the mass-transfer resistance between the bubble and cloud phases and considering the cloud as part of the bubble phase. The exchange of gaseous species was accordingly simplified to be between the bubble and the dense phases, as has been done before (Drinkenburg and Rieteura, 1972; Bukur et al., 1974; Youn and Park, 1989; Rhee and Sohn, 1990b).
2. Fresh rutile particles are fed continuously and mixed with existing particles instantaneously. They react with the gases while being dragged up by the bubbles and descending in the emulsion, and leave the bed either by overflow pipe or by entrainment by the gases.
3. The gas compositions in the bubble and emulsion phases change with bed height, but the solids are uniformly mixed throughout the bed.
4. The horizontal variation of gas concentrations in each phase can be neglected.
5. The bed is operated under an isothermal condition due to the rapid mixing in the bed.

Mass balance in the gas phase

The gases flow through the bubble and emulsion phases while exchanging mass between the phases. The gas-phase mass balances in these two phases can be expressed as follows:

$$-f_{g,b}U_b\frac{dC_{Ab}}{dZ} = \delta K_{be}(C_{Ab}-C_{Ae}) + f_{g,b}(-r_{g,b}) \quad (1)$$

$$-f_{g,e}U_e\frac{dC_{Ae}}{dZ} = \delta K_{be}(C_{Ae}-C_{Ab}) + f_{g,e}(-r_{g,e}) \quad (2)$$

where δ, the fraction of the bed volume occupied by the bubbles, is given by (Kunii and Levenspiel, 1991),

$$\delta = \begin{cases} \dfrac{U_0-U_{mf}}{U_b+U_{mf}} & \text{when} \quad U_b \cong \dfrac{U_{mf}}{\epsilon_{mf}} \\ \dfrac{U_0-U_{mf}}{U_b} & \text{when} \quad U_b \cong 5\dfrac{U_{mf}}{\epsilon_{mf}} \end{cases} \quad (3)$$

and $r_{i,j}$ is the consumption rate of reactant gas i per unit volume of the fluidized bed at a particular height in phase j. Other symbols are defined in the Notation.

The rate expression for the chlorination of rutile was experimentally determined as follows (Zhou, 1994):

$$\frac{dr}{dt} = -k_v(RT)^{1.29}C_{CO}^{0.55}C_{Cl_2}^{0.74}. \quad (4)$$

The reaction rate of rutile solid per unit surface area, R_b, has the following relation with the preceding rate expression,

$$R_b = \rho_s\frac{dr}{dt}. \quad (5)$$

From the stoichiometry of rutile chlorination reaction,

$$TiO_2(s)+2CO(g)+2Cl_2(g) = TiCl_4(g)+2CO_2(g), \quad (6)$$

the consumption rate of each gas reactant per unit area of rutile particle surface, R_a, has the following relation with R_b,

$$R_a = 2R_b. \quad (7)$$

Substituting the reaction rate expression,

$$R_a = -2k_v\rho_s(RT)^{1.29}C_{CO}^{0.55}C_{Cl_2}^{0.74}. \quad (8)$$

The gas-phase mass-balance equations, Eqs. 1 and 2, together with Eq. 8 can be applied to either CO or Cl_2. Since the volume change in the gas phase for reaction 6, especially in the presence of a carrier gas (nitrogen), is small, its effect was neglected in this work.

Mass balance for solid

The following derivation of solid-phase mass balance largely follows the development of Kunii and Levenspiel (1968, 1991). The mathematical model developed in this work, however, considers the separate variations of the gas concentrations in the bubble and emulsion phases with bed height.

The particle shrinkage rate in the bubble assemblage model is defined as

$$\Re(C,r) = \frac{dr}{dt}. \tag{9}$$

(It is noted that, in the current system, $\Re$ is independent of r, but there are other reaction systems in which it depends on r.)

With the assumption of steady state and perfect mixing of solid particles in the bed, an overall mass balance of the solid gives (Kunii and Levenspiel, 1968; Levenspiel et al., 1968)

$$F_0 - F_1 - F_2 = \sum_{\text{all } r} \left(\begin{array}{c} \text{rate of solid consumption in} \\ \text{size interval } r \text{ to } r+dr \\ \text{in the whole bed} \end{array} \right) \tag{10}$$

and

$$\left(\begin{array}{c} \text{Rate of mass} \\ \text{consumption in} \\ \text{the size interval} \\ r \text{ to } r+dr \\ \text{per unit volume} \\ \text{of the bed} \end{array} \right) = \left(\begin{array}{c} \text{rate of mass} \\ \text{consumption in} \\ \text{the size interval} \\ r \text{ to } r+dr \\ \text{in bubble phase} \\ \text{per unit volume} \\ \text{of the bed} \end{array} \right) + \left(\begin{array}{c} \text{rate of mass} \\ \text{consumption in} \\ \text{the size interval} \\ r \text{ to } r+dr \\ \text{in emulsion phase} \\ \text{per unit volume} \\ \text{of the bed} \end{array} \right). \tag{11}$$

In the bubble phase,

$$\left(\begin{array}{c} \text{Rate of mass} \\ \text{consumption in} \\ \text{the size interval} \\ r \text{ to } r+dr \\ \text{in bubble phase} \\ \text{per unit volume} \\ \text{of the bed} \end{array} \right) = \rho \left(\begin{array}{c} \text{number of} \\ \text{particles in the} \\ \text{interval} \\ r \text{ to } r+dr \\ \text{in bubble phase} \\ \text{per unit volume} \\ \text{of the bed} \end{array} \right) \left(\begin{array}{c} \text{rate of} \\ \text{volume} \\ \text{decrease for} \\ \text{one particle} \\ \text{in bubble} \\ \text{phase} \end{array} \right)$$

$$= \rho \left(\frac{y_b w P_1(r) dr}{\rho \left(\frac{4}{3} \pi r^3 \right)} \frac{dV}{dt} \right). \tag{12}$$

In the preceding equations, F_0 is the feed rate of solids with a particle-size density function of $P_0(r)$; F_1 is the withdrawal rate of solids with a particle-size density function of $P_1(r)$; F_2 is the elutriation rate of solids with a particle-size density function of $P_2(r)$; ρ is the mass density of solid; y_b is the fraction of the entire solid present in the bubble phase; w is the solid weight per unit volume of the bed; r is the particle radius, and V is the volume of a particle. Replacing dV by $4\pi r^2 dr$ and substituting the particle shrinkage rate expression,

$$\left(\begin{array}{c} \text{Rate of mass consumption} \\ \text{in the size interval} \\ r \text{ to } r+dr \\ \text{in bubble phase per} \\ \text{unit volume of the bed} \end{array} \right) = \frac{3 y_b w P_1(r)\, \Re(C_b, r)}{r} dr. \tag{13}$$

Similarly, for the emulsion phase,

$$\left(\begin{array}{c} \text{Rate of mass consumption} \\ \text{in the size interval} \\ r \text{ to } r+dr \\ \text{in emulsion phase per} \\ \text{unit volume of the bed} \end{array} \right) = \frac{3 y_e w P_1(r)\, \Re(C_e, r)}{r} dr. \tag{14}$$

Substituting Eqs. 13 and 14 into Eq. 11 and integrating along the bed height,

$$\left(\begin{array}{c} \text{Rate of mass consumption} \\ \text{in the size interval} \\ r \text{ to } r+dr \\ \text{in the whole bed} \end{array} \right) = \left[\int_0^{Hf} \frac{3 w A P_1(r)[y_b\, \Re(C_b, r) + y_e\, \Re(C_e, r)]}{r} dz \right] dr. \tag{15}$$

Substituting Eq. 15 into Eq. 10,

$$F_0 - F_1 - F_2 = \int_{\text{all } r} \left[\int_0^{Hf} \frac{3 w A P_1(r)[y_b\, \Re(C_b, r) + y_e\, \Re(C_e, r)]}{r} dz \right] dr. \tag{16}$$

The mass balance of solid in the particle-size interval r to $r+dr$ in terms of rate gives,

$$\left(\begin{array}{c} \text{Solids} \\ \text{entering in} \\ \text{the feed} \end{array} \right) - \left(\begin{array}{c} \text{solids} \\ \text{leaving in} \\ \text{overflow} \end{array} \right) - \left(\begin{array}{c} \text{solids} \\ \text{leaving in} \\ \text{carryover} \end{array} \right) + \left[\left(\begin{array}{c} \text{solids} \\ \text{shrinking into} \\ \text{the interval} \\ \text{from a} \\ \text{larger size} \end{array} \right) - \left(\begin{array}{c} \text{solids} \\ \text{shrinking out} \\ \text{of the} \\ \text{interval to a} \\ \text{smaller size} \end{array} \right) \right] - \left(\begin{array}{c} \text{solid consumption} \\ \text{due to the} \\ \text{shrinkage within} \\ \text{the interval} \end{array} \right) = 0. \tag{17}$$

All terms in Eq. 17 are straightforward, except the fourth and fifth terms. In time interval Δt, the size increment dr is determined by the fact that all the particles with the size $r+dr$, which have the shrinkage rate of dr/dt, fall into the size interval $r \rightarrow r+dr$ within the time interval dt. Thus, the fourth term has the expression,

$$dr = \frac{dr}{dt} \cdot dt = \mathfrak{R}(C,r) \cdot dt. \tag{18}$$

Therefore, in terms of rate,

$$\begin{pmatrix} \text{Solids shrinking} \\ \text{into the interval} \\ \text{from a large} \\ \text{size } r+dr \text{ in} \\ dz \text{ bed height} \end{pmatrix} = \begin{pmatrix} \text{solid shrinking} \\ \text{into the interval} \\ \text{from a large size} \\ \text{in } dz \text{ bed height} \\ \text{in bubble phase} \end{pmatrix} + \begin{pmatrix} \text{solids shrinking} \\ \text{into the interval} \\ \text{from a large size} \\ \text{in } dz \text{ bed height} \\ \text{in emulsion phase} \end{pmatrix} = wA\,dz P_1(r) y_b\, \mathfrak{R}(C_b,r) + wA\,dz P_1(r) y_e\, \mathfrak{R}(C_e,r). \tag{19}$$

Substituting Eq. 19 and other terms into Eq. 17,

$$F_0 P_0(r)dr - F_1 P_1(r)dr - F_2 P_2(r)dr + \int_0^{Hf} wAP_1(r)(y_b\, \mathfrak{R}(C_b,r) + y_e\, \mathfrak{R}(C_e,r))dz|_{r+dr} - \int_0^{Hf} wAP_1(r)(y_b\, \mathfrak{R}(C_b,r) + y_e\, \mathfrak{R}(C_e,r))dz|_r - \frac{3wAP_1(r)\,dr}{r} \int_0^{Hf} (y_b\, \mathfrak{R}(C_b,r) + y_e\, \mathfrak{R}(C_e,r))dz = 0. \tag{20}$$

The elutriation constant is defined as (Kunii and Levenspiel, 1991),

$$\kappa(r) = \frac{F_2 P_2(r)}{wAH_f P_1(r)} \tag{21}$$

and is calculated from the correlation developed by Wen and Chen (1982). Letting

$$\mathfrak{R}_t(C,r) \equiv \int_0^{Hf} [y_b\, \mathfrak{R}(C_b,r) + y_e\, \mathfrak{R}(C_e,r)]\,dz \tag{22}$$

and substituting it together with Eq. 21 into Eq. 20, one obtains

$$F_0 P_0(r) - F_1 P_1(r) - wAH_f \kappa(r) P_1(r) + wA \frac{d[\,\mathfrak{R}_t(C,r) P_1(r)]}{dr} - \frac{3wAP_1(r)\,\mathfrak{R}_t(C,r)}{r} = 0 \tag{23}$$

Single-Size Feed. For a single-size feed of radius r_m, the particle size will be less than or equal to r_m in the bed. In the size interval r to $r+dr$,

$$0 - F_1 P_1(r) - wAH_f \kappa(r) P_1(r) + wAP_1(r) \frac{d[\,\mathfrak{R}_t(C,r)]}{dr} + wA\,\mathfrak{R}_t(C,r) \frac{dP_1(r)}{dr} - \frac{3wAP_1(r)\,\mathfrak{R}_t(C,r)}{r} = 0. \tag{24}$$

Rearranging, separating, and integrating from r to r_m, one obtains

$$\ln \frac{P_1(r)}{P_1(r_m)} = 3 \ln \frac{r}{r_m} - \ln \frac{\mathfrak{R}_t(C,r)}{\mathfrak{R}_t(C,r_m)} - \int_r^{r_m} \frac{\frac{F_1}{w} + \kappa(r)}{\mathfrak{R}_t(C,r)} dr. \tag{25}$$

To evaluate $P_1(r_m)$ we take an interval r to $r+dr$ that includes r_m. For shrinking solids, no large particles shrink into this interval, so the fourth term in Eq. 20 is zero. Thus, one has

$$F_0 - 0 - 0 + 0 - wA\,\mathfrak{R}_t(C,r) P_1(r_m) - 0 = 0 \tag{26}$$

or

$$P_1(r_m) = \frac{F_0}{w\,\mathfrak{R}_t(C,r_m)}. \tag{27}$$

Substituting Eq. 27 into Eq. 25 and rearranging the equation, one obtains the particle size density function in both the bed ($P_1(r)$) and the elutriation ($P_2(r)$). First,

$$P_1(r) = \frac{F_0}{wA\,\mathfrak{R}_t(C,r)} \left(\frac{r}{r_m}\right)^3 I(r,r_m), \tag{28}$$

where

$$I(r,r_m) = \exp\left(\int_r^{r_m} \frac{\frac{F_1}{wA} + H_f \kappa(r)}{\mathfrak{R}_t(C,r)} dr \right) \tag{29}$$

and $P_2(r)$ is obtained from Eq. 21. The property of $P_1(r)$ that

$$\int_{\text{all } r} P_1(r)\,dr = 1 \tag{30}$$

gives the overall material balance relating the amount of solid per unit volume of the bed and the flow rate of mass entering the bed,

$$\frac{w}{F_0} = \int_0^{r_m} \frac{r^3}{A|R_f(C,r)|r_m^3} I(r,r_m)\,dr. \tag{31}$$

Now let us evaluate $r_{i,j}$, the consumption rate of reactant gas i per unit volume of fluidized-bed in phase j.

$$P_1(\bar{r}_i)=\frac{F_0P_0(\bar{r}_i)\Delta r_i - wA\,\mathfrak{R}_t(C,\bar{r}_{i+1})P_1(\bar{r}_{i+1})}{-wA\,\mathfrak{R}_t(C,\bar{r}_{i+1})+F_1\Delta r_i+wAH_f\kappa(\bar{r}_i)\Delta r_i-\dfrac{3wA\,\mathfrak{R}_t(C,\bar{r}_i)}{r_i}\Delta r_i} \tag{35}$$

$$\begin{pmatrix}\text{Gas consumed by}\\ \text{solids in size}\\ r \text{ to } r+dr\\ \text{in phase } j \text{ in}\\ \text{unit volume}\\ \text{of the bed}\end{pmatrix}=\begin{pmatrix}\text{number of}\\ \text{particles in size}\\ r \text{ to } r+dr\\ \text{in phase } j\end{pmatrix}\begin{pmatrix}\text{amount of gas}\\ \text{consumed by}\\ \text{one particle that}\\ \text{has the radius } r\end{pmatrix}$$

$$=\frac{y_j wP_1(r)dr}{\frac{4}{3}\pi r^3}4\pi r^2R_{a,j}$$

$$=\frac{3y_j wP_1(r)R_{a,j}\,dr}{r}. \tag{32}$$

Therefore,

$$r_{i,j}=\begin{pmatrix}\text{gas consumed by}\\ \text{solid in phase } j \text{ in}\\ \text{unit volume of bed}\end{pmatrix}=\int_0^{r_m}\frac{3y_j wP_1(r)R_{a,j}dr}{r}. \tag{33}$$

Equation 33 is combined with the mass balance for gases as shown in Eqs. 1 and 2 to solve for the reactant gas concentrations along the fluidized-bed height.

Feed of Wide Size Distribution. Levenspiel et al. (1968) derived a general equation for the solid balance based upon continuous particle-size distributions. Substituting the discrete increments of solid particles into their equation and simply changing the integral into the summation may lead to very large errors because of possible numerical inaccuracies in the required calculations. In this case, Kunii and Levenspiel (1991) suggested using the numerical procedure recommended by Overturf and Kayihan (1979), which was applied in the following derivation.

Discretizing the basic differential form of materials balance, Eq. 23 can be rewritten as

$$wA[\,\mathfrak{R}_t(C,\bar{r})P_1(\bar{r})|_{r_{i+1}}-\mathfrak{R}_t(C,\bar{r})P_1(\bar{r})|_{\bar{r}_i}]$$

$$=\left[F_0P_0(\bar{r}_i)-F_1P_1(\bar{r}_i)-wAH_f\kappa(\bar{r}_i)P_1(\bar{r}_i)-\frac{3wAP_1(\bar{r}_i)\,\mathfrak{R}_t(C,\bar{r}_i)}{\bar{r}_i}\right]\Delta r_i. \tag{34}$$

Solving for $P_1(\bar{r}_i)$, we get

and $P_1(\bar{r}_i)$ must satisfy the condition

$$\Sigma P_1(\bar{r}_i)\Delta r_i=1. \tag{36}$$

Using the materials balance, F_2 at steady state can be computed from

$$F_1+F_2-F_0=3w\sum_{i=1}^{n}\frac{P_1(\bar{r}_i)\,\mathfrak{R}_t(C,\bar{r}_i)}{\bar{r}_i}\Delta r_i. \tag{37}$$

The particle-size distribution in the elutriation stream can be evaluated by

$$P_2(r_i)=\frac{\kappa(r_i)wAH_fP_1(r_i)}{F_2}. \tag{38}$$

Equations 34 through 38 are combined with the mass balance for the gas, Eqs. 1 and 2, to obtain the particle-size distribution and gas concentrations in the bed for a wide size feed.

Heat balance

It is assumed that the temperature is uniform ($T_g \simeq T_s$) throughout the bed because of the rapid gas–solid heat transfer and solid mixing, and there is no heat accumulation. The heat balance can then be expressed as

$$\begin{pmatrix}\text{Heat}\\ \text{generated}\\ \text{by reaction}\end{pmatrix}=\begin{pmatrix}\text{heat}\\ \text{gained}\\ \text{by gas}\end{pmatrix}+\begin{pmatrix}\text{heat}\\ \text{gained}\\ \text{by solid}\end{pmatrix}+\begin{pmatrix}\text{heat}\\ \text{transferred}\\ \text{to wall}\end{pmatrix}. \tag{39}$$

In mathematical symbols,

$$AU_0(C_{A,\text{in}}-C_{A,\text{out}})(-\Delta H_r)=\bar{C}_{ps}(F_1+F_2)(T_s-T_{\text{ref}})-\bar{C}_{ps}F_0(T_{s,\text{in}}-T_{\text{ref}})+\bar{C}_{pg,\text{out}}G_{\text{out}}(T_s-T_{\text{ref}})-\bar{C}_{pg,\text{in}}G_{\text{in}}(T_{g,\text{in}}-T_{\text{ref}})+h_wA_w(T_s-T_w). \tag{40}$$

Solving these two equations, we have

$$T_s=T_{\text{ref}}+\frac{AU_0(C_{A,\text{in}}-C_{A,\text{out}})(-\Delta H_r)+\bar{C}_{ps}F_0(T_{s,\text{in}}-T_{\text{ref}})+\bar{C}_{pg,\text{in}}G_{\text{in}}(T_{g,\text{in}}-T_{\text{ref}})+h_wA_w(T_w-T_{\text{ref}})}{\bar{C}_{ps}(F_1+F_2)+\bar{C}_{pg,\text{out}}G_{\text{out}}+h_wA_w}. \tag{41}$$

For a steady-state operation, the operating temperature can be calculated from Eq. 41 using the known values of entering stream temperature and flow rate.

Method of Solution

The flow diagram for solving above equations is shown in Figure 2. There are two iteration loops in the diagram; the first is for the solid and gas balances, Eqs. 10 through 13, or Eqs. 34 to 38, and Eqs. 1 and 2, and the second is for the heat balance, Eq. 41. Unless otherwise indicated, all the model parameters were calculated based on the operating conditions using relationships given in references listed in Table 1.

To start the calculation, the initial values of the reaction temperature, CO and Cl_2 concentrations, and the particle-size distribution in the bed are assumed. For a given feed rate F_0 and to maintain the steady state, the withdrawal rate F_1 is calculated from Eqs. 29 through 31 for a single-size feed and from Eqs. 37 and 38 for a feed with a wide size distribution. The elutriation rate F_2 is evaluated from Eqs. 16 and 37, respectively. The particle-size distribution in the bed and in the elutriation is calculated using Eqs. 28 and 21 for a single-size feed and Eqs. 37 and 40 for a feed with a wide size distribution. Using the particle-size distribution in the bed thus obtained, the consumption rate of reactant gases in unit volume of the bed in either the bubble or emulsion phase is calculated by Eq. 33. Equations 1 and 2 are solved to obtain the reactant gas compositions along the bed height using the fourth-order Runge-Kutta method with adaptive step-size control (Press et al., 1987). Iterations are continued until the predetermined convergence criterion is met. The reaction temperature is obtained by solving Eqs. 43 and 44. This calculation process continues until the difference between the assumed and calculated temperature becomes smaller than a predetermined value.

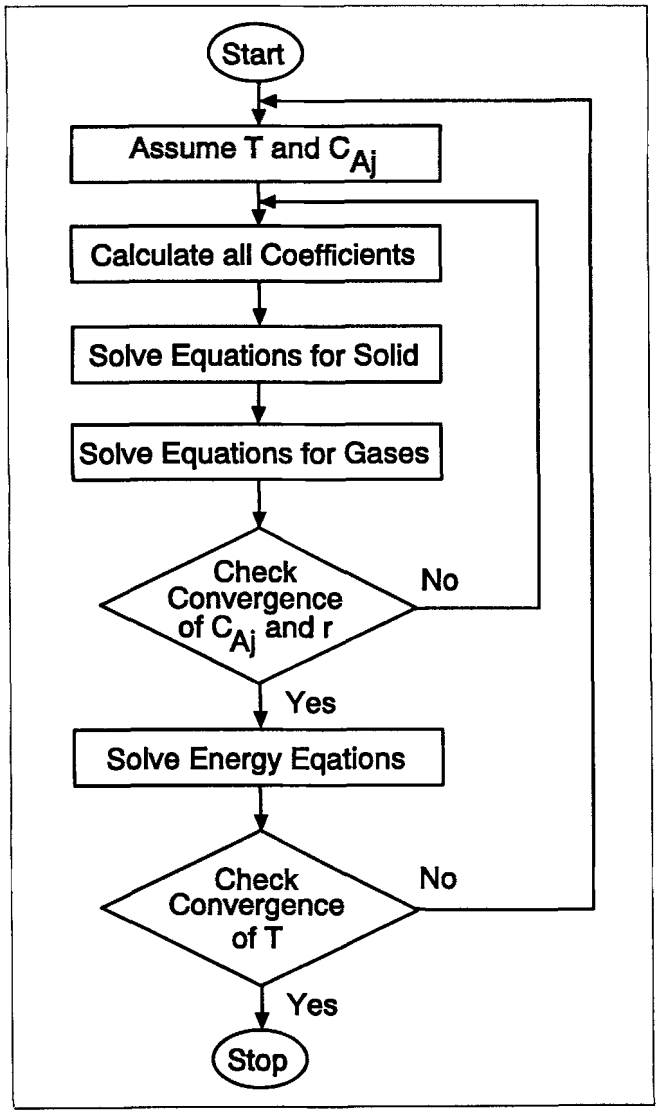

Figure 2. Flowsheet of the computer program.

Table 1. Parameter Values and Sources of Calculation Methods*

Parameter	Reference
C_{ps}	Pankratz et al. (1984)
$f_{i,j}$	Rhee and Sohn (1990b)
h_w	Kunii and Levenspiel (1991, Chap. 9)
H_f	Kunii and Levenspiel (1991, Chap. 3)
k_v	$2.39\times10^{-4}\exp(-21050/T)$ (Zhou, 1993)
u_{mf}	Kunii and Levenspiel (1991, Chap. 3)
$\kappa(r)$	Wen and Chen (1982)

*Specific gravity of TiO_2 = 4.26; atmospheric pressure = 86.1 kPa (Salt Lake City); ϵ_{mf} = 0.4 (Kunii and Levenspiel (1991, Chap. 3)).

Experimental Studies

Natural rutile used in the experiment was provided by the Du Pont company. It contained 94.4% TiO_2. The chlorination of rutile was carried out in a fluidized-bed reactor that consisted of a gas inlet system, a quartz reactor, and a product gas cooling system. A diagram of the experimental apparatus is shown in Figure 3. The fluidized-bed reactor consisted of a 2.5-cm-diameter and 95-cm-length quartz tube that had an expansion zone at the upper part to reduce the carryover to reactant particles. A coarse fritted disc was used as a bed supporter and a gas distributor. The reactor was externally heated in a silicon-carbide furnace. The temperature of the bed was measured by a thermocouple immersed in the bed. The product gases were cooled while they passed through a water-cooled condenser and bubbled through two vessels containing 10% sodium hydroxide solution. The unabsorbed chlorine was removed in an additional caustic spray tower.

The experimental procedure was to preheat the reactor to the desired temperature, flow nitrogen for 5 min to remove the oxygen in the system, place the preweighed materials while a flow of nitrogen was maintained at 900 cm^3/min at 25°C and 86.1 kPa (the atmospheric pressure at Salt Lake City). When the temperature was stabilized, the reactant gases were introduced. At the end of each experiment, the reactor was purged with nitrogen while cooling, and the quartz reactor was taken out and cooled to room temperature. The remaining sample was subjected to chemical analysis.

Results and Discussions

It is difficult to establish a steady-state chlorination condition in a laboratory, mainly because of the small equipment

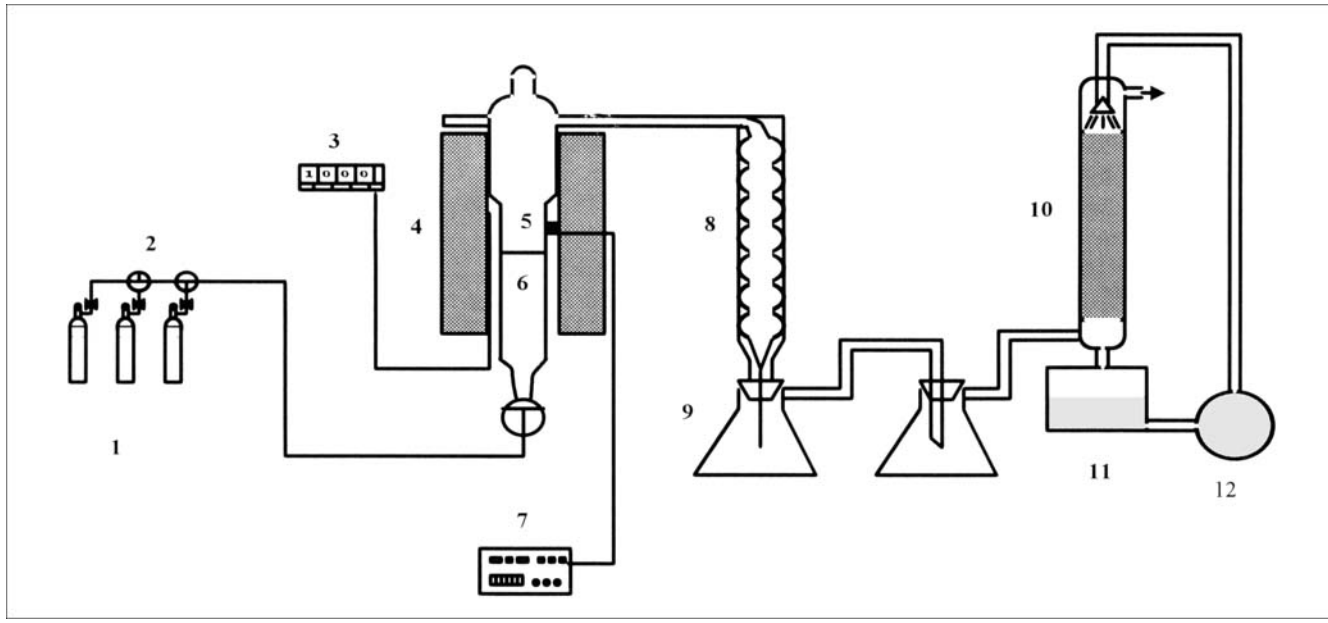

Figure 3. Diagram of experimental apparatus.

1. Gas cylinders; 2. rotameter; 3. multimeter; 4. furnace; 5. solid reactant; 6. gas distributor; 7. temperature controller; 8. cooling tube; 9. NaOH scrubber; 10. NaOH quench tower; 11. reservoir; 12. pump.

size and solid feed rate. To verify the mathematical model, batch experiments were carried out using a deep bed across which significant changes in gas concentrations occurred. Since the gas-phase dynamics are much faster than changes in the solid particles, the steady-state model was applied to each time increment, yielding the solid-particle-size distribution and the amount of solids remaining in the bed at various time increments. This is equivalent to the familiar pseudo-steady-state approximation applied to the analysis of gas–solid reactions (Szekely et al., 1976).

The most important variables affecting the performance of the bed and the reaction rate are superficial gas velocity and the exchange rate of gases between phases. In general, both chemical and hydrodynamic factors should be considered in elucidating the reactor performance (Chavarice and Grace, 1975; Fryer and Potter, 1975; Grace, 1974). The mathematical model was tested by comparing the computed results with the results of experiments under carefully selected conditions in which both the chlorination kinetics and mass-transfer effects play a significant role. This way, generally valid verification of the model can be obtained.

According to Macllvried and Massoth (1973), the effect of particle-size distribution on the overall conversion rate of solid can be represented by using the rate of conversion of the mass-average-size particle. Therefore, with the known feed particle-size distribution, the amount of reactant gases consumed in a certain time interval can be calculated based on this average rate, which in turn gives the amount of solid reacted. Thus, the decrease in particle size and the new particle-size distribution in the bed can be calculated based on the fact that particles shrink at a constant linear rate under the same reactant gas concentrations.

A number of parameters must be known to obtain numerical results. Parameter values and the sources of calculation methods for other parameters are listed in Table 1.

The predictions based on the model and the experimental results for various combinations of reacting gases for different particle-size distributions are compared in Figures 4 and 5. The experimentally controlled wall temperature in these experiments was 1,050°C. Because of the rapid solid mixing in the fluidized bed and the relatively slow chlorination reaction, the calculated gas and solid temperature were within 20°C of T_w. Thus, the system can be considered essentially isothermal. The previously formulated model is seen to be in

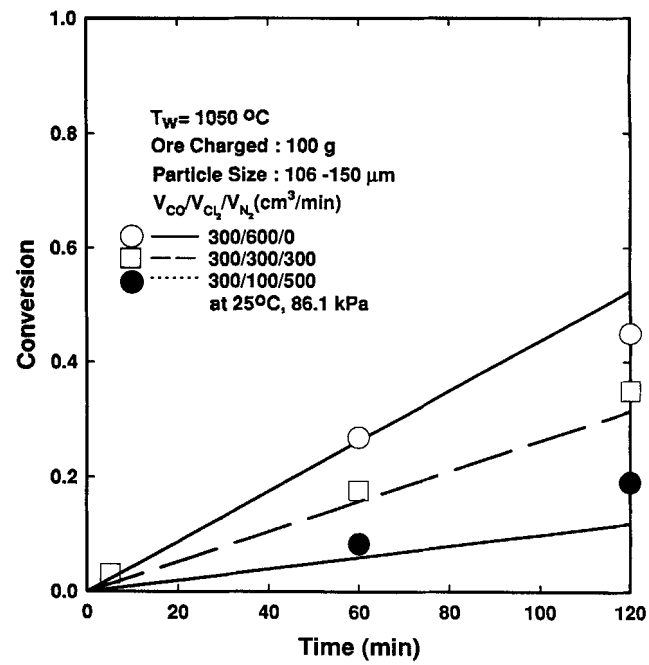

Figure 4. Experimental data vs. model prediction for a single-size feed.

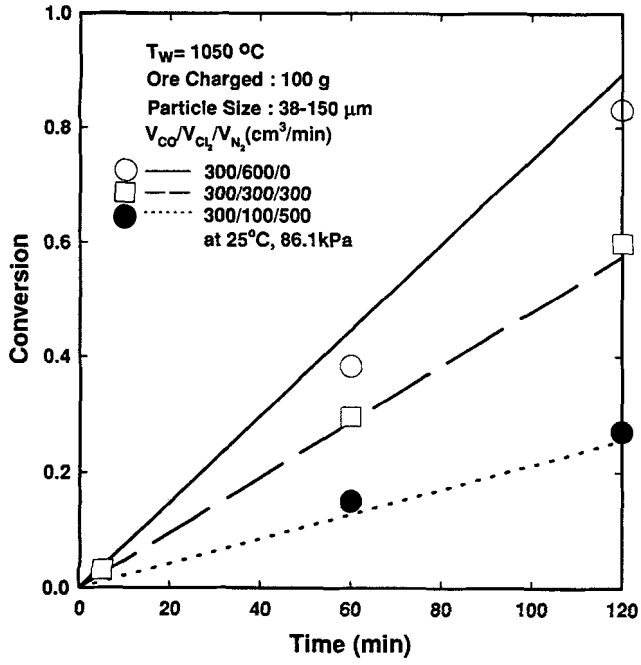

Figure 5. Experimental data vs. model prediction for a feed with a wide size distribution (feed particle-size distribution can be found in Figure 10).

good agreement with the experimental data in terms of overall conversion vs. time.

Figure 6 shows the concentration profiles for CO and Cl_2 along the bed height in the two phases. When the inlet gas contains an equimolar mixture of CO and Cl_2, the concentrations in the bubble phase are almost identical, but they are slightly different in emulsion phase, where most of the reaction takes place, due to their different diffusivities. The substantial changes in the gas concentrations along the bed height indicate that mass transfer plays an important role under the simulation conditions.

Effect of superficial gas velocity

Figure 7 shows, for a single-size feed, the concentration profiles of carbon monoxide gas in the bubble and emulsion phases along the bed height for various gas flow rates. Generally, the concentration in each phase increases with increasing flow rate. Gas velocities in the bubble and emulsion phases (U_b and U_e) increase with increasing linear velocity (U_0). The gas exchange coefficient (K_{be}) between the two phases increases with increasing gas velocity in the bubble phase and decreases due to the increase in the bubble size. At the bottom part of the bed, the gas exchange coefficient is more strongly affected by gas velocity in the bubble due to the limited bubble size. The effect of superficial gas velocity on particle-size density function in the bed and the elutriation is shown in Figure 8. Superficial gas velocity does not have much influence on the particle-size distribution in the bed, but it does affect the density function in the elutriation. From Wen and Chen's (1982) correlation, the elutriation constant and the terminal velocity in the bed increase with increasing linear gas velocity, thus increasing the sizes of the particles in the elutriation.

Concentration profiles along the bed height for various superficial gas velocities for a feed with a wide size distribution (Figure 10) show a similar trend, as illustrated in Figure 9. The differences of reactant gas concentrations between two phases decrease with an increasing superficial gas velocity.

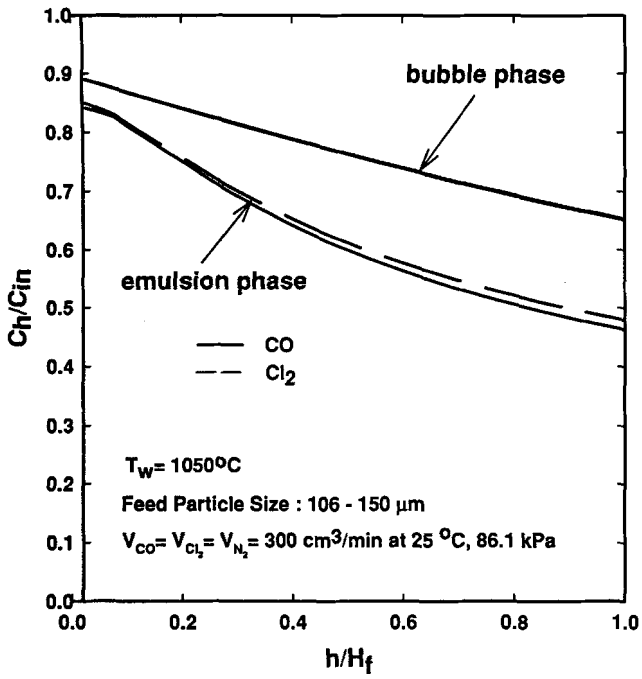

Figure 6. Calculated CO and Cl_2 concentrations along a bed height in the two phases.

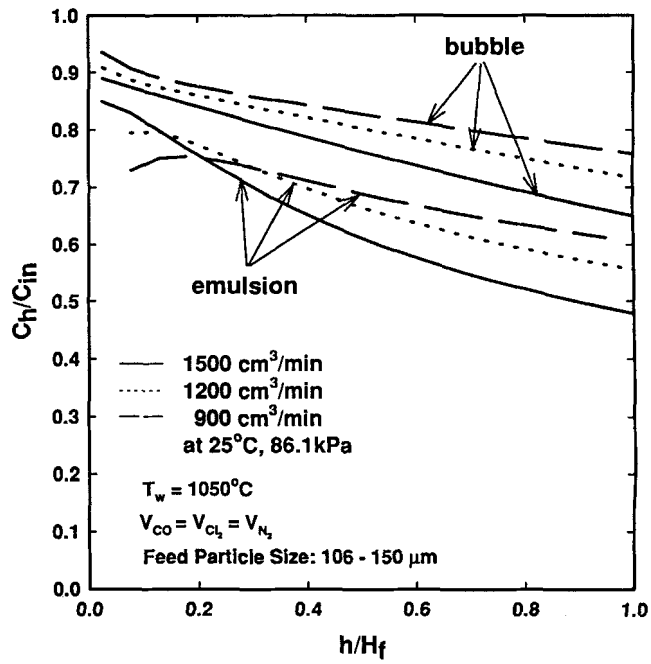

Figure 7. Calculated CO concentration along the bed height for single-size feed for various flow rates of the inlet gas.

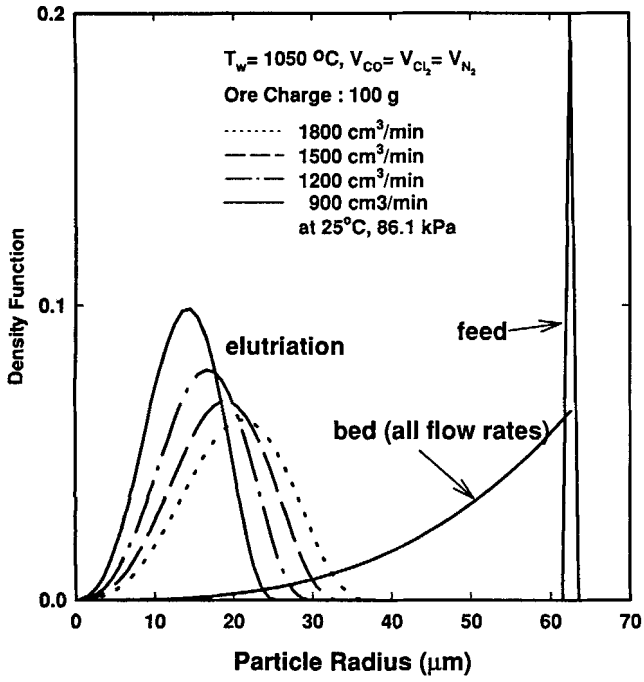

Figure 8. Particle-size density function in the bed and elutriation for single-size feed for various flow rates of steady state and no solid withdrawal except by elutriation.

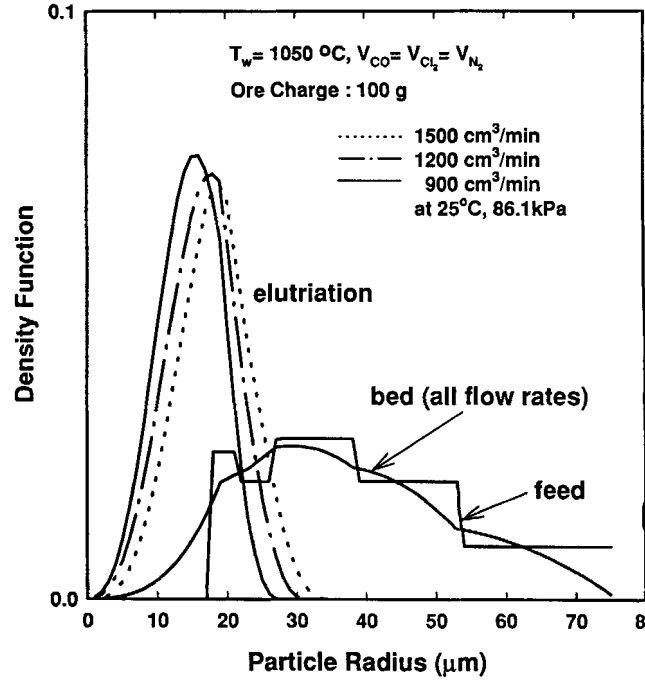

Figure 10. Particle-size density function in the bed and elutriation for a feed of wide size distribution.

This effect is more prominent in the case of a wide-size feed than for a single-size feed.

Figure 10 shows the particle-size density function in both the bed and the elutriation under various superficial gas velocities for a feed with a wide size distribution. As in the single-size feed case, the particle-size density function does not change with superficial gas velocity, but the particle size in the elutriation increases with an increasing superficial gas velocity, as expected.

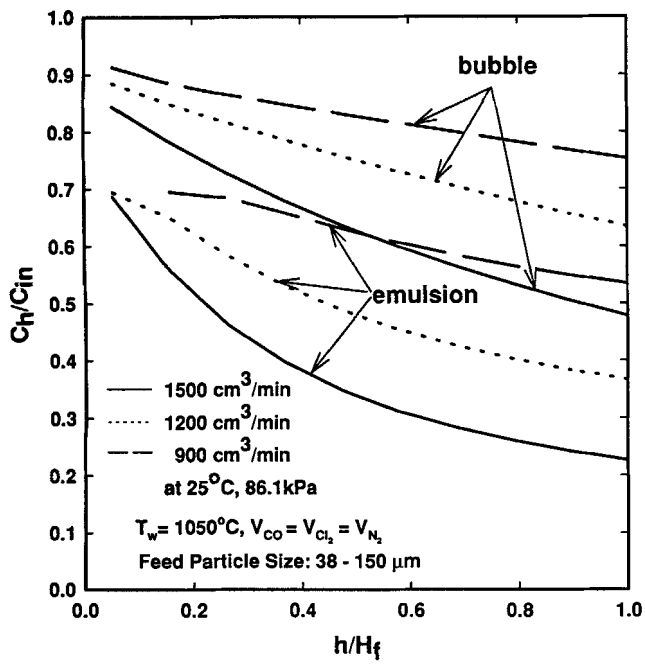

Figure 9. Calculated CO concentrations along the bed height for various gas flow rates for a feed of wide size distribution.

Effect of gas exchange coefficient

Gas exchange rate is a very important factor for the design and scale-up of a fluidized bed reactor. Its value must be evaluated by carefully considering the fluidization mode. Several different correlations have been proposed for this interchange coefficient (Chiba and Kobayashi, 1972; Drinkenburg and Rieteura, 1972). In this work, the correlation by Kunii and Levenspiel (1991) was used. Figure 11 shows the concentration profiles with different gas interchange coefficients. The reactant-gas concentration increases substantially in the emulsion phase and decreases in the bubble phase with increasing gas interchange coefficient. This effect indicates the importance of the gas interchange process and the need for a reliable method for the estimation of the exchange coefficient.

Effect of reaction-rate constant

Figure 12 shows the changes of CO concentration profiles with different reaction-rate constants. According to this figure, the CO concentration in each phase decreases with increasing reaction-rate constant, while the difference in CO concentration between the two phases increases with increasing reaction-rate constant.

This effect indicates the important role played by chemical kinetics, in addition to the mass-transfer processes, under the simulated conditions. Thus, it can be stated that the mathematical model verification shown in Figures 4 and 5 is valid

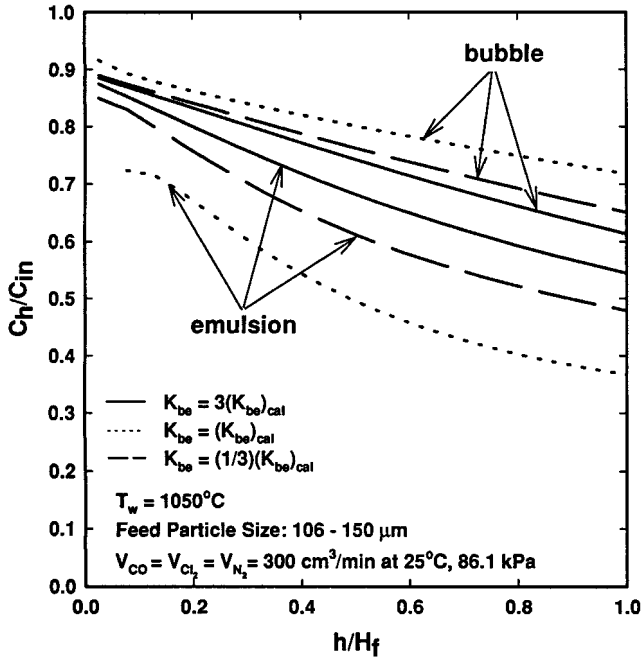

Figure 11. Calculated CO concentration profiles along the bed height for various gas interchange coefficients.

in general for different relative importance of chemical kinetics and mass-transfer effects.

Conclusions

Based on the two-phase model of a fluidized bed and the population balance of solid particles, a steady-state model was formulated to describe the overall chlorination rate, the concentration profiles of reactant gases along the bed height, the particle-size density function in the bed, and the elutriation rate of fine particles for the fluidized-bed chlorination process. The steady-state model was applied to the batch fluidized-bed chlorination by applying the pseudo-steady-state approximation. Computed results thus obtained agree well with the experimental results obtained in a deep fluidized bed for both a uniformly sized feed and a feed with a wide size distribution. The effects of superficial gas velocity, gas exchange coefficient between the bubble and emulsion phases, and reaction-rate constant on the performance of the bed were evaluated. This evaluation confirmed that the model was verified in the general case where both chemical kinetics and mass transfer are important. It further indicated the importance of correctly estimating the coefficient of gas exchange between the bubble and emulsion phases, in addition to the need for reliable kinetics information.

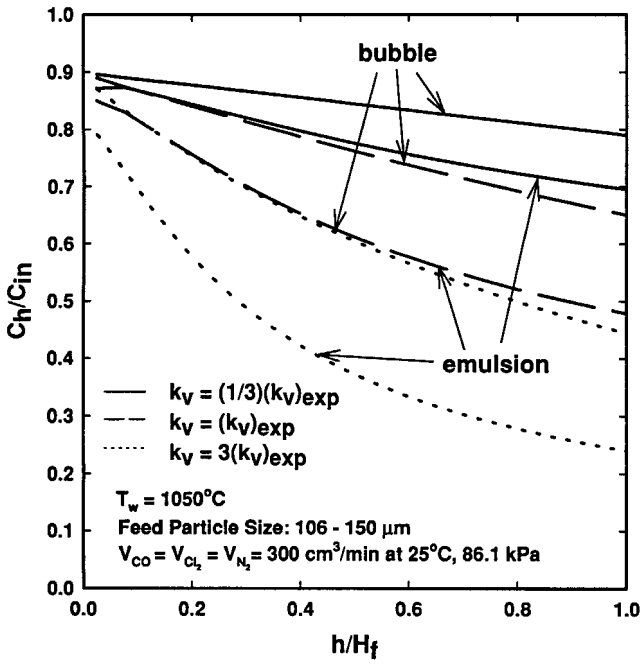

Figure 12. Calculated CO concentration profiles along the bed height for various chemical-reaction-rate constants.

Acknowledgments

Financial support by Du Pont Chemicals through unrestricted research grants and by the Department of the Interior's Mineral Institute's program administered by the Bureau of Mines under allotment grant Nos. G1114149 and G1124149 is also gratefully acknowledged. During the course of this work, one of the authors (L. Z.) received a University of Utah Graduate Research Fellowship. The authors wish to thank Drs. G. K. Whiting, P. C. Compo, and K. J. Leary of Du Pont Chemicals for supplying materials and many valuable discussions during the course of this work.

Notation

a = specific surface area (particle surface area/volume of bed), m^{-1}
A = cross-sectional area of the bed, m^2
A_w = wall area of the containing vessel, m^2
$C_{A,in}, C_{A,out}$ = concentration of reactant gas in the inlet and outlet streams, respectively, $mol \cdot m^{-3}$
C_{Aj} = concentration of reactant gas A in phase j, $mol \cdot m^{-3}$
$C_{pg,in}$ = mean heat capacity of inlet gas, $J \cdot kg^{-1} \cdot K^{-1}$
$C_{pg,out}$ = mean heat capacity of outlet gas, $J \cdot kg^{-1} \cdot K^{-1}$
C_{ps} = heat capacity of solid, $J \cdot kg^{-1} \cdot K^{-1}$
d_b = bubble diameter as a function of bed height, m
d_p = particle diameter, m
D_0 = bed diameter, m
$f_{i,j}$ = fraction of the bed volume occupied by i in phase j
G_{in} = mass rate of inlet gas, $kg \cdot s^{-1}$
G_{out} = mass rate of outlet gas that can be calculated from the conversion and stoichiometric equation, $kg \cdot s^{-1}$
h_w = heat-transfer coefficient between the bed and wall, $J \cdot m^{-2} \cdot s^{-1} \cdot K^{-1}$
H_f = fluidized-bed height, m
$(-\Delta H_r)$ = heat of reaction, J/mol of CO or Cl_2
k_v = reaction-rate constant, $m \cdot s^{-1} \cdot kPa^{-1.29}$
R = universal gas constant, 83.1 $m^3 \cdot kPa \cdot mol^{-1} \cdot K^{-1}$
T_{ref} = reference temperature or assumed temperature, K
T_w = wall temperature, K
W = bed weight, kg
y_e = fraction of entire solid present in the emulsion phase, $y_e = 1 - y_b$
z = vertical distance from the bottom of the bed, m

Greek letters

α = volumetric ratio of wake to bubble
ϵ_{mf} = voidage at the minimum fluidization
$\kappa(r)$ = elutriation constant, s^{-1}
ρ_s = true molar density of the solid, $mol \cdot m^{-3}$

Subscripts

A = CO or Cl_2
b = bubble phase
e = emulsion phase
mf = minimum fluidization

Literature Cited

Bukur, D. B., C. V. Wittmana, and N. R. Amundson, "Analysis of a Model for a Nonisothermal Continuous Fluidized Bed Catalytic Reactor," *Chem. Eng. Sci.*, **29**, 1173 (1974).

Chavarice, C., and J. R. Grace, "Performance Analysis of a Fluidized Bed Reactor," *Ind. Eng. Chem. Fund.*, **14**, 75 (1975).

Chiba, T., and H. Kobayashi, "Gas Exchange between the Bubble and Emulsion Phases in Gas-Solid Fluidized Beds," *Chem. Eng. Sci.*, **27**, 1375 (1972).

Davidson, J. F., R. Clift, and D. Harrison, *Fluidization*, Academic Press, Orlando, FL, p. 73 (1985).

Drinkenburg, A. A. H., and K. Rieteura, "Gas Transfer from Bubble in a Fluidized Bed to the Dense Phase," *Chem. Eng. Sci.*, **27**, 1765 (1972).

Fryer, C. C., and O. E. Potter, "Experimental Investigation of Models for Fluidized Bed Catalytic Reactors," *AIChE J.*, **22**, 38 (1975).

Fuwa, A., E. Kimura, and S. Fukushima, "Kinetics of Iron Chlorination of Roasted Ilmenite Ore, Fe_2TiO_5 in a Fluidized Bed," *Metall. Trans. B*, **9B**, 643 (1978).

Grace, J. R., "Fluidization and Its Application to Coal Treatment and Applied Processes," *AIChE Symp. Ser.*, **70**(141), 21 (1974).

Harris, H. M., A. W. Henderson, and T. T. Campbell, "Fluidized Coke-Bed Chlorination of Ilmenites," U.S. Bureau of Mines, RI 8165 (1976).

Kato, K., and C. Y. Wen, "Bubble Assemblage Model for Fluidized Bed Catalytic Reactors," *Chem. Eng. Sci.*, **24**, 1351 (1969).

Kunii, D., and O. Levenspiel, "Bubbling Bed Model for Kinetic Process in Fluidized Beds. Gas-Solid Mass and Heat Transfer and Catalytic Reactions," *Ind. Eng. Chem., Process Des. Develop.*, 7, 481 (1968).

Kunii, D., and O. Levenspiel, *Fluidization Engineering*, Wiley, New York, pp. 156, 254, 301, 340, 346 (1991).

Lapidus, L., and N. R. Amundson, *Chemical Reactor Theory, A Review*, Prentice Hall, Englewood Cliffs, NJ, p. 584 (1977).

Levenspiel, O., D. Kunii, and T. Fitzgerald, "The Processing of Solids of Changing Size in Bubbling Fluidized Beds," *Powder Technol.*, **2**, 87 (1968).

Macllvried, H. G., and F. E. Massoth, "Effect of Particle Size Distribution on Gas-Solid Reaction Kinetics for Spherical Particles," *Ind. Eng. Chem. Fund.*, **12**, 225 (1973).

Overturf, B. W., and F. Kayihan, "Computations for Discrete Cut Particle Size Distributions in a Fluidized Bed Reactor," *Powder Technol.*, **23**, 143 (1979).

Pankratz, L. B., J. M. Stuve, and N. A. Gokcen, *Thermodynamic Data for Mineral Technology*, U.S. Bureau of Mines Bull. 677, p. 289 (1984).

Press, W. H., B. P. Flannery, S. A. Teukolsky, and W. T. Vettering, *Numerical Recipes*, Cambridge Univ. Press, New York, pp. 283, 550 (1987).

Rhee, K. I., and H. Y. Sohn, "The Selective Chlorination of Iron from Ilmenite Ore by CO-CL_2 Mixtures: Part I. Intrinsic Kinetics," *Metall. Trans. B*, **21B**, 321 (1990a).

Rhee, K. I., and H. Y. Sohn, "The Selective Chlorination of Iron from Ilmenite Ore by CO-CL_2 Mixtures: Part II. Mathematical Modeling of Fluidized Bed Process," *Met. Trans. B*, **21B**, 331 (1990b).

Rhee, K. I., and H. Y. Sohn, "The Selective Carbochlorination of Iron from Titaniferous Magnetite Ore in a Fluidized Bed," *Metall. Trans. B*, **21B**, 341 (1990c).

Szekely, J., J. W. Evans, and H. Y. Sohn, *Gas-Solid Reactions*, Academic Press, New York (1976).

Van Swaaij, W. P. M., and F. J. Zuiderweg, "Investigation of Ozone Decomposition in Fluidized Bed on the Basis of a Two Phase Model," *Chem. React. Eng., Proc. Eur. Symp.*, **B9**, 25 (1972).

Wen, C. Y., and L. H. Chen, "Fluidized Bed Freeboard Phenomena: Entrainment and Elutriation," *AIChE J.*, **28**, 117 (1982).

Werther, J., "Scale-Up of Fluidized Bed Reactors," *Ger. Chem. Eng.*, **1**, 243 (1978).

Youn, I.-J., and K. Y. Park, "Modeling of Fluidized Bed Chlorination of Rutile," *Metall. Trans. B*, **20B**, 959 (1989).

Zhou, L., "Fluidized Bed Chlorination of Several Titaniferous Materials—Kinetics, Morphological Changes and Mathematical Modeling," PhD Diss., Univ. of Utah, Salt Lake City, p. 63 (1994).

Manuscript received Sept. 19, 1995, and revision received May 3, 1996.